Astron. Astrophys. 339, 208–214 (1998)

ASTRONOMY AND ASTROPHYSICS

Broadening of Si VIII lines observed in the solar polar coronal holes

D. Banerjee[1], **L. Teriaca**[1], **J.G. Doyle**[1], **and K. Wilhelm**[2]

[1] Armagh Observatory, College Hill, Armagh BT61 9DG, Northern Ireland (dipu@star.arm.ac.uk; lte@star.arm.ac.uk; jgd@star.arm.ac.uk)
[2] Max-Planck-Institut für Aeronomie, D-37191 Katlenburg-Lindau, Germany (wilhelm@linmpi.mpg.de)

Received 15 April 1998 / Accepted 27 July 1998

Abstract. We study the variation of the line width and electron density as a function of height above two coronal holes from forbidden spectral lines of Si VIII. The spectra were obtained with the Solar Ultraviolet Measurements of Emitted Radiation spectrometer flown on the *Solar and Heliospheric Observatory* spacecraft. The observations concentrate on the dark regions outside the plumes, which are believed to be the locations, where the fast solar wind originates. The line width data show that the non-thermal line-of-sight velocity increases from 27 $\mathrm{km\ s^{-1}}$ at 27 arc sec above the limb to 46 $\mathrm{km\ s^{-1}}$ some 250 arc sec (i.e. ∼180,000 km) above the limb. The electron density shows a decrease from 1.1 10^8 $\mathrm{cm^{-3}}$ to 1.6 10^7 $\mathrm{cm^{-3}}$ over the same distance. This data implies that the non-thermal velocity is inversely proportional to the quadratic root of the electron density, in excellent agreement with that predicted for undamped radially propagating Alfvén waves. We show that the energy flux associated with these hydromagnetic waves is sufficient to drive the high speed solar wind streams.

Key words: Sun: corona – waves – Sun: UV radiation

1. Introduction

Doschek & Feldman (1977) measured line profiles of forbidden lines and inferred non-thermal velocities between 17 and 25 km $\mathrm{s^{-1}}$ at altitudes of 10–20 arc sec above a coronal hole and several 'quiet' Sun regions. Based on SKYLAB data, Doschek et al. (1977), Nicolas et al. (1977) and Mariska et al. (1978) have shown that the line width increases with height above the limb. These earlier observations were restricted to temperatures in or below the transition region and thus inferring details concerning coronal heating was not possible. Hassler et al. (1990) obtained line profile data for the coronal lines Mg X 609/625 Å up to ∼ 140,000 km above the limb. Recently Doyle et al. (1998) showed an increase in line width up to ∼ 70,000 km above the limb for 'quiet' Sun conditions at the equatorial Western limb. Such data has important implications for deciding the merits of the different coronal heating mechanisms. This paper provides observational evidence suggesting that a significant energy flux may be transported by Alfvén waves in the solar polar coronal holes.

To isolate line broadening due to hydromagnetic waves, it is necessary to observe the line widths of high temperature coronal lines (∼ 10^6 K) above the limb. With the launch of SOHO, and in particular with the, SUMER instrument (Wilhelm et al. 1995), line width measurements of coronal lines as a function of position above the limb are possible. Here, we report an observational sequence involving the Si VIII line pair (1445.75 Å & 1440.49 Å). Observations of this line pair allows us to determine simultaneously the electron density and the line width.

Recently Doschek et al. (1997) have used some of the same datasets, although they determined only the electron densities. We go one step further, measuring the line widths along with the electron density. Wilhelm et al. (1998) also have determined electron densities in coronal holes, but their main interests were on the electron temperature estimates in polar plumes and inter-plume lanes. Ulysses observations have indicated that fast solar wind originates from polar coronal holes. During the year 1996, part of the minimum sunspot activity, the polar coronal holes were well developed and relatively stable. This gives us the ideal opportunity to study the fast solar wind acceleration site, namely the polar coronal holes. Koutchmy & Bocchialini (1997) and Wilhelm et al. (1998) have suggested that the source of the fast solar wind lies in the low density background plasma (and not the plumes). So in this study we concentrate on the darkest region outside plumes, namely the inter-plume lanes (see Fig. 1). Our objective is to infer the cause of the line width variation, plus the possible role of waves on coronal heating and the driving of the solar wind.

2. Observations and data reduction

SUMER is a normal incidence spectrograph operating over the wavelength range 400 Å to 1610 Å. The off-axis parabola mirror is moveable in two dimensions around the focal point allowing pointing of the instrument independent of the spacecraft altitude. Four slits are available; 4×300, 1×300, 1×120 and 0.3×120 $\mathrm{arcsec^2}$. For the data obtained here we used the 4×300(slit 1) and 1×300(slit 2) $\mathrm{arc\ sec^2}$ slits. The detectors (see Siegmund et al. 1994) have 1024 spectral pixels and 360 spatial pixels, each. The central area is coated with KBr which increases the

Send offprint requests to: D. Banerjee

Table 1. SUMER Polar coronal hole observations, N(S)PCH = north(south) polar coronal hole. Slit 1,2 = 4x300, 1x300 arc sec^2 respectively.

Date	Region	Detector	Slit	Solar X-Y Co-Ord	Starting time	End Time	Exp. Time (s)	No. of spectra
4 Nov'96	NPCH	B	2	0,+1107	04:54	10:36	320	63
10 Dec'96	NPCH	B	1	0,+1229	03:30	09:11	320	68
5 May'96	SPCH	A	2	0,−1100	03:46	04:18	320	6

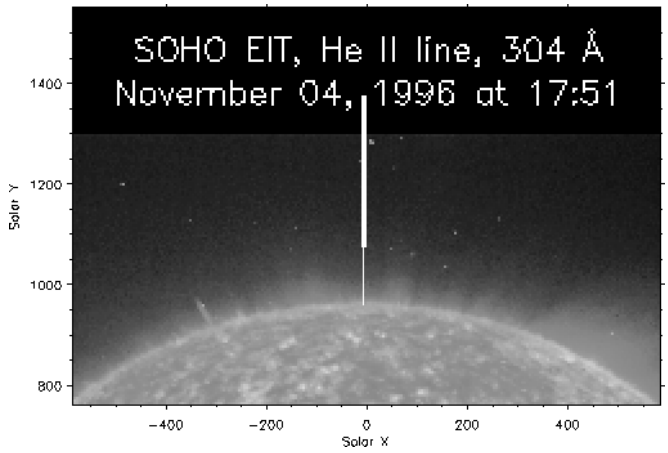

Fig. 1. The locations for slit 1 (on Dec 10) & slit 2 (on Nov 4) datasets in the north coronal hole on an EIT image (courtesy of the EIT consortium) of He II 304 Å obtained on 4th November, 1996 at 17:51 UT.

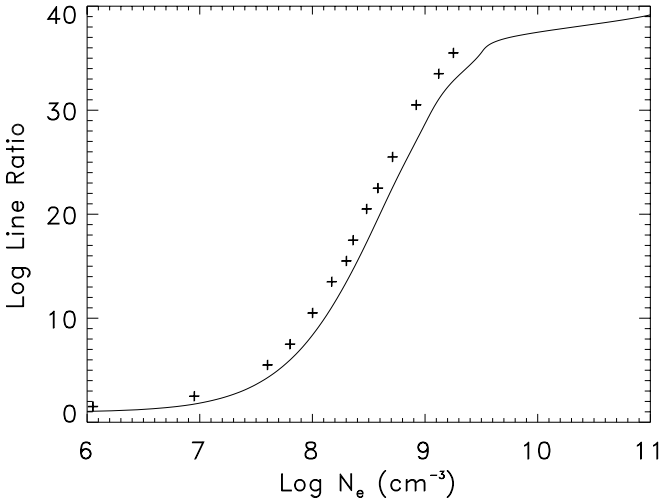

Fig. 2. Density dependence of the Si VIII line ratio (1445.75 Å/1440.49 Å) for the atomic data within CHIANTI (solid line) and for comparison the ratios given by Doschek et al. (1997) (+).

quantum efficiency by up to an order of magnitude in the range 900 Å to 1500 Å. The dates of observations, locations, pointing positions of the centre of the slits, slit sizes and exposure times are given in Table 1. The slits were, for a nominal spacecraft orientation, oriented in the north-south direction parallel to the solar radius. The spatial resolution (1 arc sec $\sim$ 715 km) along the slit provides the intensities as a function of height outside the limb. For the observation in the north polar coronal hole (NPCH) we used two sequences of temporal serial images (i.e. a series of spectra taken in the same pointing position but at successive times). All the images taken with the same slit and at the same location were summed resulting in two final spectra relating to the NPCH and one for the south polar coronal hole (SPCH). Details on the total number of individual spectra used is given in Table 1. The objective of the observing programme was to obtain high S/N spectra of the Si VIII 1440.49 Å and 1445.75 Å lines as a function of position in the N(S)PCH. Fig. 1 shows an image of the North polar region taken with EIT in He II 304 Å at 17:51 UT on November 4, 1996 with the slit 1 & 2 locations superimposed. Note that the slits are positioned in the darkest region of NPCH, in the inter-plume lanes. We have also checked, with the EIT images on May 5, 1996, that for the SPCH, the pointing of the slit was in the inter-plume region.

The inference of the electron density in an ionized plasma using the line ratio of forbidden lines of higher ions like Si VIII has been used by several authors, e.g. Feldman et al. (1978), Doschek et al. (1997), Wilhelm et al. (1997) and Doyle et al. (1998). Fig. 2 shows the variation of the Si VIII line intensity ratio as a function of electron density obtained from the CHIANTI atomic data base (Dere et al. 1997). The (+) symbols indicate the values used by Doschek et al. (1997). This figure clearly shows that the Si VIII ratio is a useful density diagnostic for densities in the range 10^7 cm^{-3} to several 10^9 cm^{-3}. For the SUMER instrument, the process of data reduction involves three main steps; destretching, radiometric calibration and slit effects corrections, which were done using various IDL routines from within the SUMER software tree (see Doyle et al. 1998 for details). The flat-fielding was done onboard the satellite.

3. Results

A Gaussian profile was fitted to each spectral line. Only data from outside the solar limb could be fitted due to the faintness of the Si VIII lines on-disk and blending problems (Doyle et al. 1998). In Fig. 3, we show sample fits to the data at 47 arc sec above the limb for slit 2 and 139 arc sec for slit 1. In all instances, both Si VIII lines can be fitted with a single Gaussian, although the 1440.39 Å line is slightly affected by the presence of a nearby line.

Table 2 summarizes the results for the N(S)PCH. Figs. 4a & 5a shows the variation of electron density above the limb, calculated from the CHIANTI data in Fig. 2. In the case of the NPCH data, the densities are derived from line profiles averaged over 10 arc sec (1 spatial detector pixel corresponds to $\sim$1 arc sec) up to 190 arc sec, with the last three data points being the

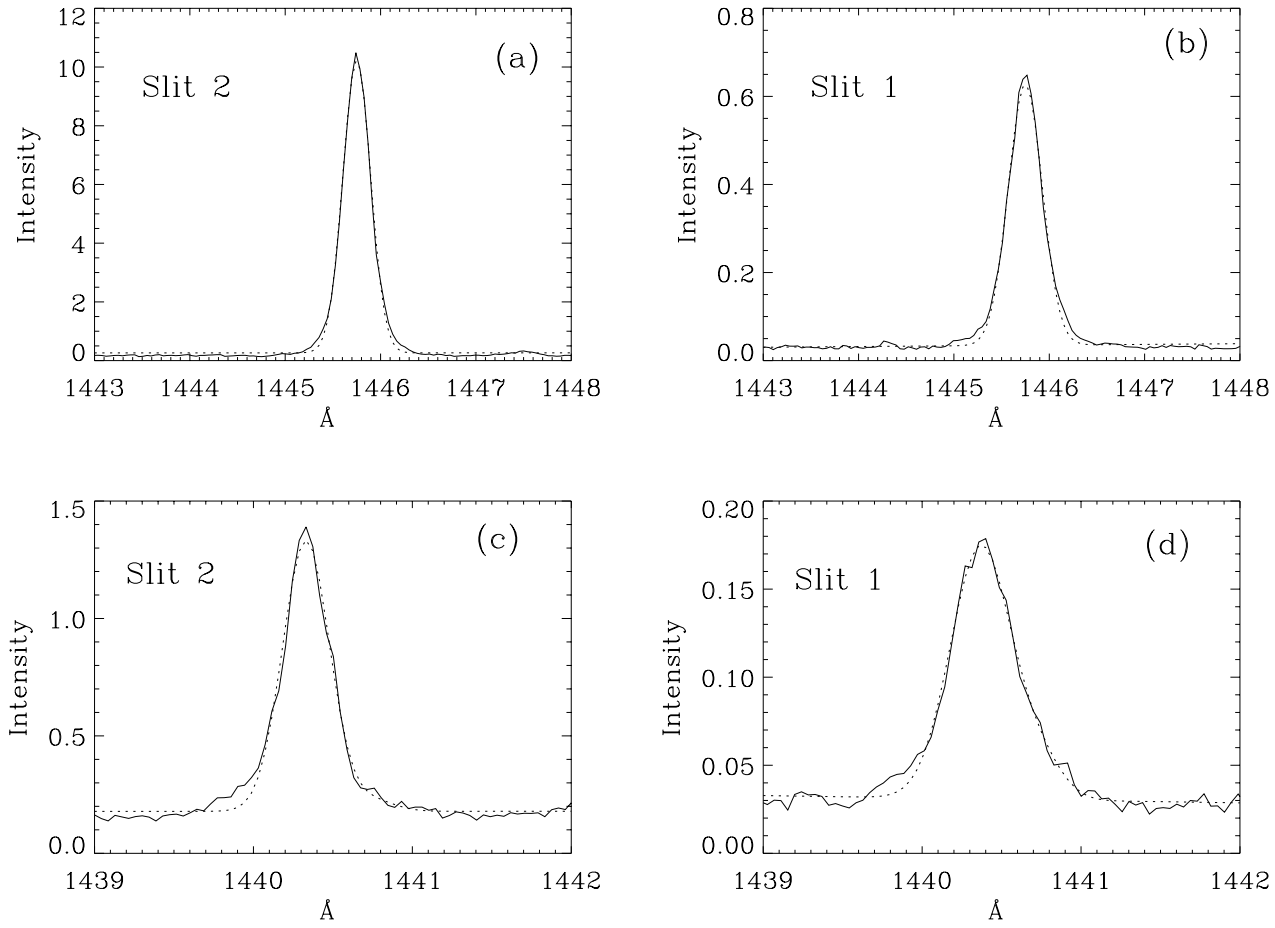

Fig. 3. a,b Sample Si VIII 1445.75 Å and **c,d** 1440.49 Å line fits to the data at 47 (**a,c**) and 139 (**b,d**) arc sec above the limb respectively (solid line are the data and the dotted line is the fit). Intensities units are in erg cm^{-2} s^{-1} sr^{-1} Å^{-1}

average of 20, 20 and 30 arc sec respectively. For the SPCH we have averaged over 20 arc sec throughout.

The error in deriving the electron density in Figs. 4a & 5a depends not only on the line strengths but also on the atomic data. The relative measuring error in deriving N_e is estimated to be 12% to 15%, similar to the expected absolute error (see Laming et al. 1997). Recently Doyle et al. (1998) measured electron densities at the equatorial limb, again using the Si VIII line ratio. Comparing their Table 1 with the present values, the densities in the coronal holes are significantly lower than the 'quite' Sun, approximately a factor of two as already noted by Doschek et al. (1997).

The spectral line profile of an optically thin line results from the thermal broadening caused by the ion temperature T_i and broadening caused by non-thermal motions. Assuming a Gaussian distribution one obtains,

$$FWHM = \left[4ln2\left(\frac{\lambda}{c}\right)^2\left(\frac{2k_BT_i}{M}+\xi^2\right)\right]^{1/2}, \qquad (1)$$

where T_i is the ion temperature, and M the ion mass. ξ is the non-thermal speed, related to the wave amplitude by $\xi^2 = \frac{1}{2} < \delta v^2 >$, where the factor of 2 accounts for the polarization and direction of propagation of a wave relative to the line of sight. The measured line profiles will also depend on the instrumental characteristics. The spectrometer will introduce an instrumental width, which is 77 mÅ($FWHM$) for detector A and 95 mÅ($FWHM$) for detector B at 1445 Å. In addition, the slit width has to be considered. The latter effect can not be treated as a Gaussian distribution and a de-convolution is required. This has been done using the standard SUMER software and the corrected values are tabulated in Table 2. The magnitude of this correction is small, although it does result in a correction in the derived non-thermal velocity of $\sim$2 km s^{-1} for slit 2 and $\sim$2.5 km s^{-1} for slit 1. Note that the formation temperature of Si VIII in ionization equilibrium is $T_e = 8\,10^5$ K. Recently Wilhelm et al. (1998) have estimated the electron temperatures in the interplume lanes of coronal holes to be $\leq 900,000$ K. They have also indicated that ions in a coronal hole are hotter than the electrons. Furthermore, observations at larger distances from the limb obtained by UVCS (Antonucci et al. 1997), demonstrate that the assumption of collisional ionization equilibrium(CIE) and the common notion that $T_i = T_e$ in the coronal hole plasma are not realistic. Tu et al. (1998) have argued that in a coronal region a few tens arc seconds above the solar limb the CIE assumption

Table 2. A summary of the measured and corrected line width for Si VIII 1445.75 Å, plus the derived non-thermal velocities (ξ) and the electron densities for N(S)PCH = north(south)polar coronal hole and slits 1,2 = 4x300, 1x300 arc sec^2 respectively, using $T_i = 1\ 10^6$ K.

Limb posn. (arc sec)	Region	Slit	I(1445.75 Å) (erg cm^{-2} s^{-1} sr^{-1})	Ratio	$FWHM$ (mÅ) Measured	Corrected	ξ (km s^{-1})	log N_e/cm^{-3}
27	NPCH	2	7.42	9.31	308	291.6	27.0	8.06
37	NPCH	2	6.87	10.31	326	310.5	30.1	8.13
47	NPCH	2	4.94	8.62	344	329.4	33.1	8.02
57	NPCH	2	3.45	8.10	348	333.6	33.7	7.98
67	NPCH	2	2.41	6.69	374	360.6	37.8	7.87
77	NPCH	2	1.78	6.24	372	358.5	37.5	7.83
87	NPCH	2	1.41	6.04	381	367.9	38.9	7.81
98	NPCH	2	1.02	5.36	382	368.9	39.0	7.74
108	NPCH	2	0.72	4.99	395	382.3	41.0	7.69
118	NPCH	2	0.57	4.82	382	368.9	39.0	7.67
119	NPCH	1	0.50	4.91	432	402.5	43.9	7.68
129	NPCH	1	0.45	4.21	445	416.5	45.8	7.59
139	NPCH	1	0.37	4.23	421	390.6	42.2	7.59
149	NPCH	1	0.27	3.88	444	415.4	45.7	7.54
159	NPCH	1	0.22	3.49	447	418.6	46.2	7.48
169	NPCH	1	0.19	3.61	442	413.3	45.4	7.50
179	NPCH	1	0.15	3.59	446	417.5	46.0	7.49
194	NPCH	1	0.11	2.80	453	425.0	47.1	7.33
219	NPCH	1	0.07	2.69	428	398.2	43.3	7.30
250	NPCH	1	0.04	2.39	449	420.8	46.5	7.22
17	SPCH	2	7.87	10.81	297	285.5	26.0	8.16
37	SPCH	2	4.03	7.94	305	293.8	27.4	7.97
57	SPCH	2	2.28	6.62	327	316.6	31.1	7.86
77	SPCH	2	1.32	5.41	360	350.6	36.3	7.74

may not apply, and therefore the ion kinetic temperatures may not have anything to do with the electron temperature or the formation temperature. To explore further, the ion temperature versus electron temperature question, we derive the non-thermal velocity (ξ) using Eq. (1), assuming three different ion temperatures, $8\ 10^5$K, $1\ 10^6$K and $2\ 10^6$K. If we assume ionization equilibrium, and use $T_i = T_e = 8\ 10^5$K, we find a set of non-thermal velocities which is marginally higher than our theoretically calculated ones (indicated by + symbols in Figs. 4b & 5b, see later). Whereas, if we use $T_i = 2\ 10^6$K, then the observed non-thermal velocities varies from ~ 10 km s^{-1} at 25 arc sec above the limb to ~ 39 km s^{-1} at 250 arc sec above the limb, which is much lower compared to our theoretical values and other observations. From the comparison of our observed dataset and theoretical implications (which will be discussed in the next section) we find $T_i = 1\ 10^6$K to be the best choice. This is consistent with the estimates given by Tu et al. (1998), who have measured the effective ion temperatures in a solar polar coronal hole observed by SUMER. Furthermore, we should remind the readers that the resultant non-thermal velocities are model-dependent. In Figs. 4b & 5b we show the variation of ξ with height above the limb for $T_i = 1\ 10^6$K. For the non-thermal velocity measurement, we have used the width of the (stronger) Si VIII 1445.75 Å line. The accuracy in the ξ measurement is around 0.5 km s^{-1} for slit 2 and around 1 km s^{-1} for slit 1. The Si VIII data indicates that for the NPCH, the non-thermal velocity increases from ~ 27 km s^{-1} at 25 arc sec above the limb to ~ 46 km s^{-1} at 250 arc sec above the limb for plasma around $1\ 10^6$ K. For the SPCH, the non-thermal velocity increase from ~ 26 km s^{-1} at 17 arc sec above the limb to ~ 36 km s^{-1} at 80 arc sec above the limb. In Figs. 4 & 5 the dashed lines are second order polynomial fits to the observed data. Note that for the last three points in Fig. 4b (beyond 200 arc sec) in the case NPCH, the uncertainty in measuring ξ is ~ 1.5 km s^{-1}. The (+) symbols are obtained from the theoretical expression (Eq. [3]). The implications of these plots will be discussed in the following section.

4. Discussion

The measurement of line widths can provide information concerning ion temperatures, sub-resolution turbulent motions and velocity fluctuations associated with magnetohydrodynamic (MHD) waves in the corona. Although a number of mechanisms, including Alfvén waves, have been shown to be consistent with previous observations (Hassler et al. 1990; Doyle et al. 1998), none of these observations of the line broadening have been done for the coronal hole regions. Doyle et al. (1998) have discussed, that purely acoustic waves are not important for coronal heating (Hollweg, 1990) and the slow and fast magnetoacoustic waves are also not able to supply the coronal energy requirements.

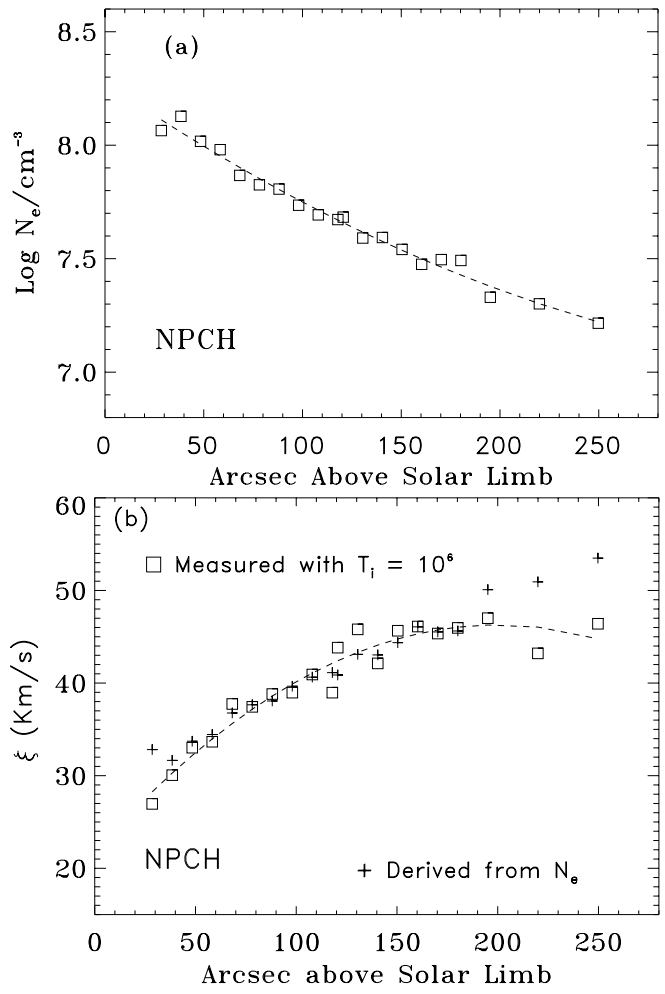

Fig. 4. a The electron density as measured via the Si VIII 1445 Å/1440 Å line ratio as a function of position above the North Polar coronal hole, **b** the non-thermal velocity as derived from Si VIII using $T_i = 1\ 10^6$ K. The dashed line is a second order polynomial fits, while the (+) symbols correspond to theoretical values (see text).

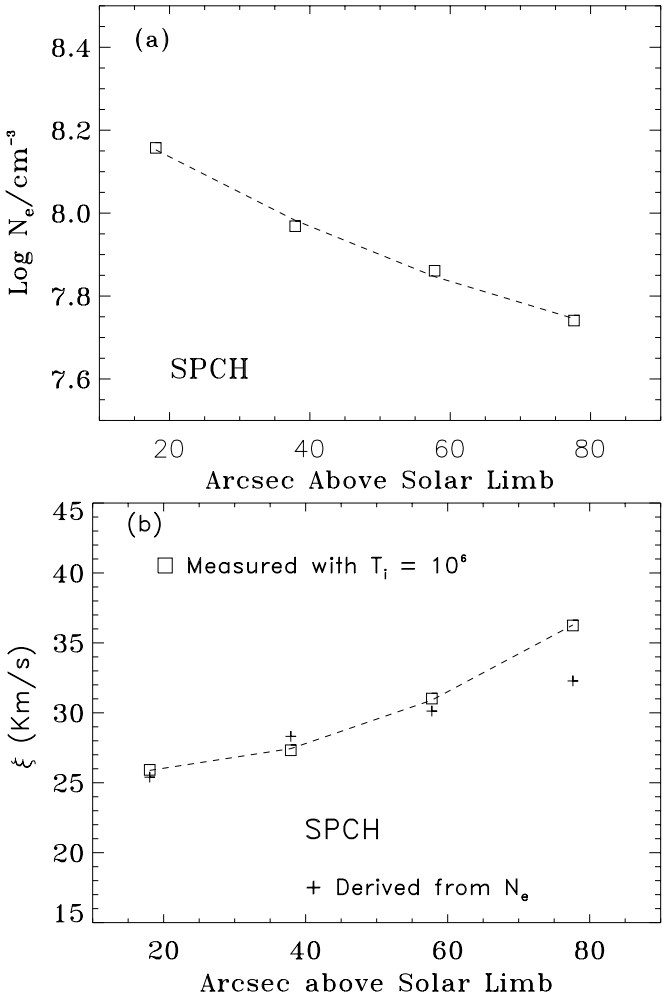

Fig. 5. a The electron density as measured via the Si VIII 1445 Å/1440 Å line ratio as a function of position above the South Polar coronal hole, **b** the non-thermal velocity as derived from Si VIII using $T_i = 1\ 10^6$ K. The dashed line is a second order polynomial fit, while the (+) symbols correspond to theoretical values (see text).

It is well known that the Alfvén waves propagate virtually undamped through the quasi-static corona and deposit their energy flux in the higher corona. Low frequency Alfvén waves are reflected in the chromosphere-corona transition region, but the higher frequency Alfvén waves with a wavelength that is shorter than the Alfvén speed scale height, may play an important role in heating coronal holes (Hollweg 1990). Axford & McKenzie (1992) first suggested that the high speed wind originates directly from the chromospheric network at the bottom of a coronal hole, and that high frequency waves at 10-10^4 Hz are possibly created there, by small scale reconnections. Based on these ideas Marsch & Tu (1997) have developed a two-fluid model and demonstrated that Alfvén waves are quite appropriate for both heating the coronal funnels through cyclotron dissipation and accelerating the wind with the help of wave pressure gradient. They have considered spatial inhomogeneity in the form of rapid expanding flux tubes, implying an increase of its cross sectional area and a decrease of magnetic field strength with height. From a parametric study they inferred that for acceleration of the solar wind the wave amplitude required are of the order of several 10 km s^{-1}, which is consistent with our observations. Thus our observations will provide initial conditions for such model calculation.

Although Parker (1958) developed the theory of solar wind acceleration, the mechanism responsible is not yet fully understood. In particular, observations of the high speed solar wind indicates the need for a substantial energy flux that is transported outward from the coronal base by some process other than convection or classical thermal conduction. Marsch & Tu (1997) have pointed out that the most natural means of energy transport guided by field lines is through the Alfvén mode and its high frequency extensions up to the local cyclotron frequency. The energy flux density in the corona due to Alfvén waves is given by (Doyle et al. 1998),

$$F = \sqrt{\frac{\rho}{4\pi}} < \delta v^2 > B \qquad (2)$$

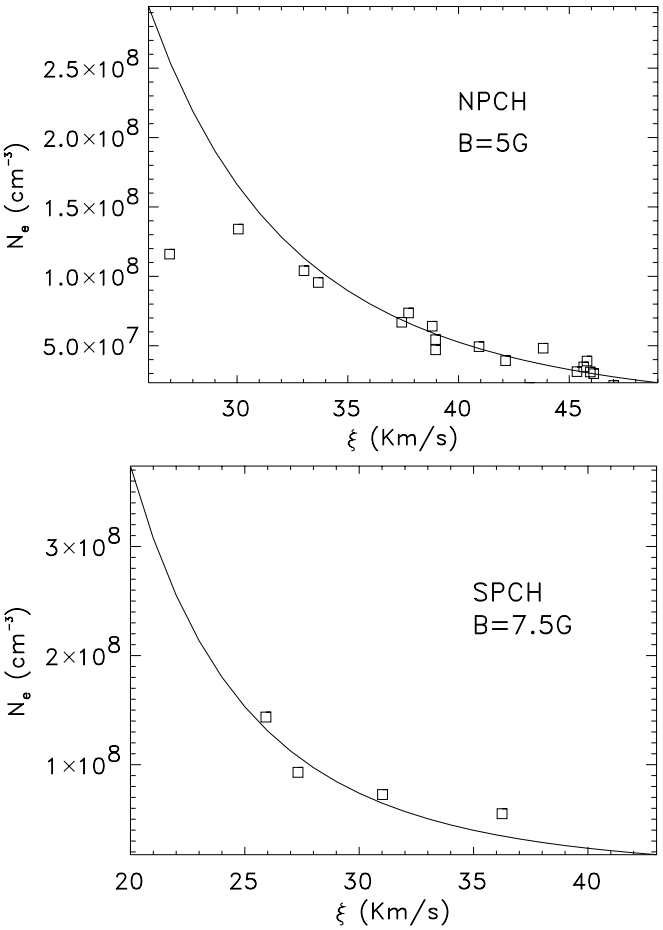

Fig. 6. Variation of electron density with non-thermal velocity for the N(S)PCH. The squared boxes represents the measured values as given in Table 2 and the solid lines represent the theoretical relation (Eq. [3]) for magnetic field strengths as indicated.

where ρ is the plasma mass density (related to N_e as $\rho = m_p N_e$, m_p is the proton mass), $< \delta v^2 >$, the mean square velocity is given previously, and B, is the magnetic field strength. From our dataset at 120 arc sec above the limb for the NPCH using $N_e = 4.8\ 10^7$ cm^{-3}, $< \delta v^2 >= 2 \times (43.9\ \mathrm{km\ s^{-1}})^2$ (see Table. 2), we find $F = 4.9\ 10^5$ erg cm^{-2} s^{-1} for $B = 5$ G, which is only sightly lower than the requirements for a coronal hole with a high speed solar wind flow (Withbroe & Noyes 1977), which is estimated to be $8\ 10^5$ erg cm^{-2} s^{-1}. The average field strength in coronal holes is estimated to be 5-10 G (Hollweg, 1990). One should note that we have used the WKB approximation. Hollweg (1990) have shown that a non-WKB approach enhances the energy flux somewhat. Furthermore, non-linear effects could also be important. Recently Torkelsson et al. (1998) have studied numerically, the propagation of nonlinear spherical Alfvén waves in a radial magnetic field. They show that the wave damps by forming current sheets, in which the Poynting flux is lost to Ohmic heating and the acceleration of an upflow. This process could be important for the fast solar wind.

Assuming that the linear analysis is correct and gives a fairly reasonable estimate of the energy flux, expression (2) shows that the rms wave velocity amplitude and density are related by,

$$< \delta v^2 >^{1/2} \propto\ \rho^{-1/4} \tag{3}$$

In Figs. 4b & 5b, the (+) represents the velocities calculated on the basis of Eq. (3), using the measured N_e. In both cases, we find excellent agreement, however in order to explore the consistency further, we show additional plots in Fig. 6. The solid lines are the theoretically predicted functional form of the variation of electron density with non-thermal velocity (Eq. [3]) and the squared boxes are the values derived from the line ratios (see Table 2). The proportionality constant have been chosen to match the calculated energy flux. For the SPCH data we have used B=7.5 G. Once again the agreement is very good. Note that the first data point in Fig. 6a corresponds to values close to the limb, thus it is possible that they are contaminated to some degree by foreground and background 'quiet' Sun emission. The other possibility is that these are affected by compressional magnetic waves which are believed to be present close to the solar limb. Lou & Rosner (1994) showed that the behaviour of the magnetic waves are very similar to that of Alfvén waves, with compressible effects falling off much more rapidly with increasing height, as compared to the Alfvén waves. Lou (1996) assumes a rough equipartition of overall wave energies associated with magnetic waves and Alfvén waves at the coronal base and estimated the velocity fluctuations to be $\sim 18 - 20$ km s^{-1}. If that is the case then the first data-point is well explained.

Using SUMER data Wilhelm et al. (1998) have obtained the electron temperatures to be less than 800,000 K in a plume in the range from r = 1.03 R$_\odot$ to 1.6 R$_\odot$ decreasing with height to $\sim$ 330,000 K. Near an inter-plume lane, they found electron temperatures between 750,000 K to 880,000 K in the same height interval, while Tu et al. (1998) have found that the ion temperature remains roughly constant. We show that for Si VIII we require an ion temperature of $1\ 10^6$K in order to obtain an excellent fit to the observed data and the theoretically calculated values (see Figs. 4b & 5b). This is only slightly larger than the Si VIII formation temperature assuming ionization equilibrium, i.e. $T_e \sim 8\ 10^5$. On the other hand, $T_i = 2\ 10^6$ is not consistent with the theory and our observations.

Applying the conservation of energy flux we can also derive a relation between the non-thermal velocity and magnetic field strength as,

$$\xi \propto B^{-1/2} \tag{4}$$

Using Eq. (4) we find that a non-thermal velocity, $\xi = 30$ km s^{-1} at 37 arc sec above the limb in a 5 G coronal hole corresponds to 1.5 km s^{-1} in a 2 KG photospheric field. This is comparable to the solar granulation velocity. Thus, this procedure also allows us to estimate roughly the magnetic field strength at different heights.

From a study of low latitude coronal streamers, Seely et al. (1997) did not find any conclusive evidence for any observable turbulent velocity at altitudes of 109 arc sec and 209 arc sec

above the equatorial limb. They argued that their result casts doubt on the heating of the corona and acceleration of the solar wind by hydromagnetic waves in the streamers. Since only the low speed wind originates from the coronal streamers, this problem is not relevant for fast wind emanating from the polar inter-plume regions. In the present study our results can consistently be explained by hydromagnetic waves in coronal holes. The observed non-thermal velocities at different heights are also consistent with upward propagating Alfvén waves. To verify the consistency further, we have looked at the line broadening of other coronal lines. Our preliminary results, which we hope to present in a subsequent paper, shows a similar trend. Furthermore our observations imposes limits on the assumed wave amplitude for the model calculation of Marsch & Tu (1997). Observed amplitudes presented here for polar coronal holes are still adequate for the requirements of coronal heating by the dissipation of high frequency Alfvén waves.

Acknowledgements. Research at Armagh Observatory is grant-aided by the Dept. of Education for N. Ireland while partial support for software and hardware is provided by the STARLINK Project which is funded by the UK PPARC. This work was supported by PPARC grant GR/K43315. We would like to thank the SUMER and EIT teams at Goddard Space Flight Center for their help in obtaining the data. The SUMER project is financially supported by DLR, CNES, NASA, and PRODEX. SUMER is part of SOHO, the Solar and Heliospheric Observatory of ESA and NASA.

References

Antonucci, E., Noci, G., Kohl, J., et al., 1997 in Advances in the Physics of Sunspots, eds. B. Schmieder, J. C. del Toro Iniesta, & M. Vazquez, ASP Conf Ser., 118, 273
Axford, W. I., and McKenzie, J. F., 1992, in Solar Wind seven, eds. E. Marsch & R. Schwenn (Oxford: Pregamon Press), 1
Dere, K.P., Landi, E., Mason, H.E., Monsignori-Fossi, B. and Young, P.R., 1997, A&A S 125, 149
Doschek, G.A., Feldman, U. and Cohen, L., 1977, ApJ S 33, 10
Doschek, G.A. and Feldman, U., 1977, ApJ 212, L143
Doschek, G.A., Warren, H.P., Laming, J.M., Mariska, J.T., Wilhelm, K., Lemaire, P., Schühle, U. and Moran, T.G.., 1997, ApJ 482, L109
Doyle, J.G., , Banerjee, D. & Perez, M.E., 1998, Sol Phys (in press)
Feldman, U., Doschek, G.A., Mariska, J.T., Bhatia, A.K. and Mason, H.E., 1978, ApJ 226, 674
Hassler, D.M., Rottman, G.J., Shoub, E,C. and Holzer, T.E., 1990, ApJ 348, L77
Hollweg, J.V., 1990, Computer Phys Reports 12, 205
Koutchmy, S., and Bocchialini, K., 1997, in Robotic exploration Close to the Sun, ed. S. R. Habbal, AIP Conf Proc 385,137
Laming, J.M., Feldman, U., Schühle, U., Lemaire, P., Curdt, W. and Wilhelm, K., 1997, ApJ 485, 911
Lou, Y.Q. and Rosner, R., 1994, ApJ 424, 429
Lou, Y.Q, 1996, MNRAS 281, 750
Mariska, J.T., Feldman, U. and Doschek, G.A., 1978, ApJ 226, 698
Marsch, E., and Tu, C.-Y., 1997, Sol Phys 176, 87
Nicolas, K.R., Brueckner, G.E., Tousey, R., Tripp, D.A., White, O.R. and Athay, R., 1977, Sol Phy 55, 305
Parker, E.N., 1958, ApJ 128, 664
Seely, J.F., Feldman, U., Schühle, U., Wilhelm, K., Curdt, W. and Lemaire, P., 1997, ApJ 484, L87
Siegmund, O.H.W., Gummin, M.A., Stock, J.M. et al., 1994, Proc SPIE 2280, 89
Torkelsson, Ulf., Boynton, G. C., 1998, MNRAS 295, 55
Tu, C.-Y., Marsch, E., Wilhelm, K., and Curdt, W., 1998, ApJ (in press)
Wilhelm, K., Curdt, W., Marsch, E. et al., 1995, Sol Phys 162, 189
Wilhelm, K., Lemaire, P., Curdt, W. et al., 1997, Sol Phys 170, 75
Wilhelm, K., Marsch, E., Dwivedi, B.N. et al., 1998, ApJ 500 (in press)
Withbroe, G.L. and Noyes, R.W., 1977, ARA&A 15, 363